Crystallographic Orientation-dependent Optical Properties of InGaSb/GaAs Quantum Well Architecture

S.M. Tasmeeh Ahsan[1], Mahmoodul Islam [1], Sourov Roy[2], Utpal Bhowmik[3]

[1]Department of Electrical and Electronic Engineering, American International University-Bangladesh
[2]Department of Electrical and Electronic Engineering, Varendra University, Rajshahi, Bangladesh
[3]Department of Electrical and Electronic Engineering, Prime University, Dhaka, Bangladesh

Abstract— A methodical approach is introduced to establish energy dispersion relation with hole sub-band states and optical gain spectra for variant growth directions such as [00 1], [1 1 0], [1 1 1], [1 1 3] and [1 1 1] of compressively strained InGaAs/GaAs quantum well (QW) architecture by solving envelope function equation using finite difference method. It is demonstrated that there is a substantial correlation between optical gain and its emission wavelength amidst a particular crystal orientation of the QW. From the MATLAB simulation results, it can be settled that the dispersion relation between hole sub-band states, optical gain, and the threshold current density in [1 1 1] direction deviates exclusively from the other directions, in particular, the more conventional [0 0 1]. The regular optical gains are inspected 2750 cm-1,3250 cm-1, 2800 cm-1, 2900 cm-1,and 1900 cm-1 in [0 0 1], [1 1 0], [1 1 1], [1 1 3], and [1 3 1] crystal orientations, respectively, when the injection carrier density is 2×10^{18} cm^{-3}. Eventually, the highest optical power and the lowest threshold current are attained in orientation [1 1 0] while the number of quantum well is five.

Keywords— Crystal orientation, Quantum well, GaInAs, Valence band, Transition momentum matrix

INTRODUCTION

A quantum well (QWs), literally a potential well with only discrete energy values, comprised of Gallium Arsenide (GaAs) and of related III-V materials exhibits appreciable current conducting performance. Consequently, its application scope broadens up to the operation as the active region in short wavelength light-emitting diodes and laser diodes. The earliest and perhaps the most established hetero-structure laser technique is AlGaAs/GaAs structure. The range of available wavelength (λ) for lattice matched AlGaAs/GaAs QW hetero-structure is from 0.80-0.65 μm. The long wavelength limit is characterized by the band-edge of substrate. Either the active layers of alloy or the quantum size effect or both are manipulated to alter the emission to the shorter wavelengths. But the range of wavelength (λ) 0.88-1.1 μm is not readily available in any III-V architecture lattice matched laser material system. There are, however, a number of important applications that require emission in this range, especially pump lasers for rare earth doped silica fiber amplifiers. In conventional optical system, a pump laser diode at wavelength 0.98 μm, an optical coupler, and a length of Erbium doped optical fiber are incorporated to form a propagating wave optical amplifier which is considered as a critical component in fiber optic communication scheme. [1-4]

A simple demonstration on direct gap III-V compound semiconductor alloys suggests[5] that, perchance, the best material system for attaining the emission wavelength in range of 0.88-1.1 μm is $In_xGa_{1-x}Sb$.There is, however, no suitable binary substrate that allows lattice matched composition of $In_xGa_{1-x}Sb$ in the wavelength range of interest. Thus, only a hetero-structure material technique in which a large lattice mismatch must be accommodated (as great as 3%) may be considered.

Recent research presents that optical gain and threshold current of lasers can be improved by introducing a compressively strained QW into the active region.[6] The band structure of the compressively strained QW firmly depends on the crystal orientations.[7] To obtain favorable band structure for higher optical gain, the disband between heavy hole (HH) and light hole (LH) should be increased and the effective mass of holes should be reduced. The disband between subbands and effective masses can be controlled by changing crystal orientations which leads to possible invention of novel electro-optic devices. Hence, crystal orientation is the unique parameter to optimize QW performance.

The growth of crystal orientated QW structure except [0 0 1] orientation is efficiently attainable by modernized crystal growth techniques such as molecular beam epitaxy and metal-organic chemical vapor deposition. The growth of high quality epitaxial layers on [2 0 1] GaAs substrates has been reported by Woolf et al. practicing the molecular beam epitaxy method. In particular on this occasion, AlAs/GaAs multilayered structures have been developed on [2 1 0] oriented substrate by Nötzel and Ploog. To avoid the structural degradation associated with non-[0 0 1] substrate, [0 0 1] orientated substrates are used with non-[0 0 1] orientated QW active region using wafer bonding technique .

In order to anticipate the optical and electronic properties of QW structures, one-dimension Schrödinger equation has most often been employed for modeling any modifications to the energy band structure of arbitrary crystal oriented QWs. Energy band structure and transition momentum matrix modifications due to change in crystal orientations are evaluated by Henderson and Towe solving Schrödinger equations.[8-9] The [100] wurtzite (WZ) crystal based QW lasers are found to have higher carrier densities to generate better optical gain because these structures not only have a large internal field due to the strain-induced piezoelectric (PZ)

and spontaneous (SP) polarizations , [10-12]but also a heavier hole effective mass than the conventional zinc-blende (ZB) crystals.[13]

To reduce the threshold carrier density in wurtzite crystal lasers, non-[100] orientation has been recently studied as an additional parameter.[14-19]In addition, Zinc-blende-type GaAs structures have also been investigated experimentally and theoretically. From theoretical aspect, several authors have studied the hole subband states and optical gains for zinc-blende [001] structure and have compared the results to those of wurtzite(001). However, only a few reports have been focused on Zinc Blende (ZB) QWs growth in other crystallographic orientation such as (1 1 0), (1 1 1), (1 1 2) and (1 1 3) [20].

In this paper, the optical and electrical properties of compressively strained zinc-blende InGaSb/GaAs QWs have been investigated by using the effective-mass theory for [001], [1 1 0], [1 1 1], [1 1 3] and [1 31] orientations. Here, 8 nm quantum well is sandwiched between 7 nm barrier layers. To inspect the optical properties of QW structures in arbitrary crystal orientation, unitary transformations are used to modify the wave vector and strain matrix. The Hamiltonian matrix in conventional [0 0 1] crystal orientation is also transformed to the arbitrary crystal orientation. The conduction and valence band wave functions and Eigen energies of the proposed QW structures are evaluated using the finite difference method. The momentum matrix element, gain spectra and injection carrier density dependent-optical gain are reckoned using the conduction and valence band energies and wave functions.

THEORY

A. *The k.p Method of Band-Structure Calculation near Γ-point:*

The electronic band structure is solved in the envelope approximation using an eight-band $\boldsymbol{k}\cdot\boldsymbol{p}$ Hamiltonian. The modified Kane 8×8 Hamiltonian matrix can be asserted by:

$$H\psi_h(z) = E\psi_h \tag{1}$$

While, H is resultant Hamiltonian matrix that can be expressed by:

$$H = H_0 + H_\varepsilon \tag{2}$$

The components of resultant Hamiltonian matrix are illustrated below:

$$H_0 = \begin{bmatrix} A & 0 & V^* & 0 & \sqrt{3}V & -\sqrt{2}U & -U & \sqrt{2}V^* \\ 0 & A & -\sqrt{2}U & -\sqrt{3}V^* & 0 & -V & \sqrt{2}V & U \\ V & -\sqrt{2}U & -P+Q & -S^* & R & 0 & \sqrt{\frac{3}{2}}S & -\sqrt{2}Q \\ 0 & -\sqrt{3}V & -S & -P-Q & 0 & R & -\sqrt{2}R & \frac{1}{\sqrt{2}}S \\ \sqrt{3}V^* & 0 & R^* & S & -P+Q & S^* & \frac{1}{\sqrt{2}}S^* & \sqrt{2}R^* \\ -\sqrt{2}U & -V^* & 0 & R^* & S & -P+Q & \sqrt{2}Q & \sqrt{\frac{3}{2}}S^* \\ -U & \sqrt{2}V^* & \sqrt{\frac{3}{2}}S^* & -\sqrt{2}R^* & \frac{1}{\sqrt{2}}S & \sqrt{2}Q & -P-\Delta & 0 \\ \sqrt{2}V & U & -\sqrt{2}Q & \frac{1}{\sqrt{2}}S^* & \sqrt{2}R & \sqrt{\frac{3}{2}}S & 0 & -P-\Delta \end{bmatrix} \tag{3}$$

$$\Psi_h(z) = \begin{Bmatrix} \Phi_{1/2,1/2}(z) \\ \Phi_{1/2,-1/2}(z) \\ \Phi_{3/2,1/2}(z) \\ \Phi_{3/2,-1/2}(z) \\ \Phi_{3/2,3/2}(z) \\ \Phi_{3/2,-3/2}(z) \\ \Phi_{1/2,1/2}(z) \\ \Phi_{1/2,-1/2}(z) \end{Bmatrix} = \begin{Bmatrix} g^{(1)}(z) \\ g^{(2)}(z) \\ g^{(3)}(z) \\ g^{(4)}(z) \\ g^{(5)}(z) \\ g^{(6)}(z) \\ g^{(7)}(z) \\ g^{(8)}(z) \end{Bmatrix} \tag{4}$$

Where, ϕ_{j,m_j} or $g^{(j)}$ is the conduction and valence band wave function component and E is the energy of conduction band and three valence bands.

The matrix elements are[21]:

$$A = E_c - \frac{\hbar^2}{2m_0}(k_x^2+k_y^2+k_z^2) \tag{5}$$

$$P = -E_v - \gamma_1\frac{\hbar^2}{2m_0}(k_x^2+k_y^2+k_z^2) \tag{6}$$

$$Q = -\gamma_2\frac{\hbar^2}{2m_0}(k_x^2+k_y^2+k_z^2) \tag{7}$$

$$R = \sqrt{3}\frac{\hbar^2}{2m_0}[\gamma_2(k_x^2 - k_y^2) - 2i\gamma_3 k_x k_y] \tag{8}$$

$$S = -\sqrt{3}\gamma_3\frac{\hbar^2}{2m_0}k_z(k_x - ik_y) \tag{9}$$

$$U = \frac{-i}{\sqrt{3}}P_0 k_z \tag{10}$$

$$V = \frac{-i}{\sqrt{6}}P_0(k_x - ik_y) \tag{11}$$

P_0 is the coupling between the conduction and valence bands, E_c and E_v are the (unstrained) conduction and valence band energies respectively, Δ is the spin orbit splitting and γ_i's are modified Luttinger parameters. The other component of the resultant Hamiltonian matrix, H_ε depicted in equation (2) is the strain Hamiltonian matrix that can be revealed by[22]:

$$H_\varepsilon = \begin{bmatrix} a_c e & 0 & -v^* & 0 & -\sqrt{3}v & \sqrt{2}u & -u & -\sqrt{2}v^* \\ 0 & a_c e & \sqrt{2}u & \sqrt{3}v^* & 0 & v & -\sqrt{2}v & -u \\ -v & \sqrt{2}u & -p+q & -s^* & r & 0 & \sqrt{\frac{3}{2}}s & -\sqrt{2}q \\ 0 & \sqrt{3}v & -s & -p-q & 0 & r & -\sqrt{2}r & \frac{1}{\sqrt{2}}s \\ \sqrt{3}v^* & 0 & r^* & s & -p-q & s^* & \frac{1}{\sqrt{2}}s^* & \sqrt{2}r^* \\ \sqrt{2}u & v^* & 0 & r^* & s & -p+q & \sqrt{2}q & \sqrt{\frac{3}{2}}s^* \\ u & -\sqrt{2}v^* & \sqrt{\frac{3}{2}}s^* & -\sqrt{2}r^* & \frac{1}{\sqrt{2}}s & \sqrt{2}q & -a_v e & 0 \\ -\sqrt{2}v & -u & -\sqrt{2}q & \frac{1}{\sqrt{2}}s^* & \sqrt{2}r & \sqrt{\frac{3}{2}}s & 0 & -a_v e \end{bmatrix}$$

The elements of H_ε matrix are:

$$p = a_v(e_{xx}+e_{yy}+e_{zz}) \tag{12}$$

$$q = b[e_{zz} - \frac{1}{2}(e_{xx}+e_{yy})] \tag{13}$$

$$r = \frac{\sqrt{3}}{2}b(e_{xx} - e_{yy}) - ide_{xy} \tag{14}$$

$$s = -d(e_{xz} - ie_{yz}) \tag{15}$$

$$u = \frac{-i}{\sqrt{3}}P_0\sum_j e_{zj}k_j \tag{16}$$

$$v = \frac{-i}{\sqrt{6}}P_0\sum_j(e_{xj} - ie_{yj})\,k_j \tag{17}$$

Here, e_{ij} is the strain tensor; a_c is the conduction band deformation potential; a_v is the valence band deformation potential; b and d are the shear deformation potentials.

The energy dispersion profile along [100] orientation is calculated as a function of k for the 8-band k.p theory by diagonalizing the Hamiltonian using finite difference scheme.

B. *Crystal orientation dependent wave vector and strain*

If the active region is grown on arbitrary crystal orientation, the wave vectors on [100] crystal can be attained by the subsequent expression[23]:

$$\begin{pmatrix} k_1 \\ k_2 \\ k_3 \end{pmatrix} = O_R \begin{pmatrix} k_x \\ k_y \\ k_z \end{pmatrix} \tag{18}$$

The strain on (100) crystal orientation can be reckoned by[23]:

$$\begin{pmatrix} \varepsilon_{11} & \varepsilon_{12} & \varepsilon_{13} \\ \varepsilon_{21} & \varepsilon_{22} & \varepsilon_{23} \\ \varepsilon_{31} & \varepsilon_{32} & \varepsilon_{33} \end{pmatrix} = O_R \begin{pmatrix} \varepsilon_{xx} & \varepsilon_{xy} & \varepsilon_{xz} \\ \varepsilon_{yx} & \varepsilon_{yy} & \varepsilon_{xz} \\ \varepsilon_{zx} & \varepsilon_{zy} & \varepsilon_{zz} \end{pmatrix} O_R{}^T \tag{19}$$

Here, $\varepsilon_{ij}(i, j = x, y, z)$ are the strain tensors in (hkl) direction. The values of diagonal elements are:

$$\varepsilon_{xx} = \varepsilon_{yy} = \varepsilon_X = (a_{well} - a_{barr})/a_{barr}$$

$$\varepsilon_{zz} = -\frac{C_{11}}{2C_{12}}\varepsilon_X$$

Here, C_{11} and C_{12} are the elastic constants of the well material and the values of off-diagonal matrix element are set to zero in case of in-plane strain condition.

The expression of the rotation matrix is as follows[24]:

$$O_R = \begin{pmatrix} \cos\theta\cos\phi & -\sin\phi & \sin\theta\cos\phi \\ \cos\theta\sin\phi & \cos\phi & \sin\theta\sin\phi \\ -\sin\theta & 0 & \cos\theta \end{pmatrix} \tag{20}$$

Where, $\theta = \tan^{-1}(\frac{\sqrt{(h^2+k^2)}}{l})$ and $\phi = \tan^{-1}(k/h)$

Practicing the wave vector in the (100) crystal orientation, the Hamiltonian matrix for [100] crystal orientation can be calculated according to section 2.2. Then the Hamiltonian matrix in (hkl) orientation can be counted by the consecutive equation[25]:

$$H^{hkl} = U H^{(100)} U^* \tag{21}$$

Where, $U = R(\theta)R(\phi)$

In this equalization, $R(\theta)$ and $R(\phi)$ are symbolized as rotations which transform the [100] orientated valence band Hamiltonian to arbitrary crystal orientated Hamiltonian matrix. The argument of $R(\theta)$ and $R(\phi)$ can be defined by:

$$R(\theta) = \begin{pmatrix} \alpha^2 & -\sqrt{3}\alpha^2\zeta & \sqrt{3}\alpha\zeta^2 & \zeta^3 \\ \sqrt{3}\alpha^2\zeta & \alpha^3 - 2\alpha\zeta^2 & -2\alpha^2\zeta + \zeta^3 & \sqrt{3}\alpha\zeta^2 \\ \sqrt{3}\alpha\zeta^2 & 2\alpha^2\zeta - \zeta^3 & \alpha^3 - 2\alpha^2\zeta & -\sqrt{3}\alpha^2\zeta \\ \zeta^3 & \sqrt{3}\alpha\zeta^2 & \sqrt{3}\alpha^2\zeta & \alpha^3 \end{pmatrix} \tag{22}$$

$$\alpha = \cos\frac{\theta}{2} \text{ and } \zeta = -\sin\frac{\theta}{2}$$

$$R(\phi) = \begin{pmatrix} e^{i(3/2)\phi} & 0 & 0 & 0 \\ 0 & e^{i(1/2)\phi} & 0 & 0 \\ 0 & 0 & e^{-i(1/2)\phi} & 0 \\ 0 & 0 & 0 & e^{-i(3/2)\phi} \end{pmatrix} \tag{23}$$

2.2) Optical gain:

The optical gain as a function of energy for quantum well architecture can be addressed by[26]:

$$g(E) = \frac{2q^2\eta}{n\varepsilon_0 cm_0{}^2 LE} \times \sum_{n,m} \int_0^\infty \frac{k_t M_{nm}(k_t)\Gamma/(2\pi)}{(E_{cn}(k_t) - E_{kpm}(k_t) - E)^2 + (\Gamma/2\pi)^2} (f_c{}^n - f_v{}^m) dk_t \tag{24}$$

Here, q is denoted as free electron charge, η as reduced Planck constant, n as the index of refraction, ε_0 as free space dielectric constant, c as speed of light, E as photon energy, E_{cn} as the n[th] conduction sub-bands, E_{kpm} as the m[th] valence sub-bands, and M_{nm} as the momentum matrix element in strained quantum well architecture. $\Gamma = \frac{\hbar}{\tau}$; τ is the photon relaxation time. F_c, F_v are the Fermi levels of conduction and valence band. The momentum matrix element for transition can be written as[26]:

$$M_{nm}(k_t) = \frac{3}{4}\left[\left\langle \psi_{n(k_t=0)} \middle| g^{(1)}{}_m \right\rangle^2 + \frac{1}{3}\left\langle \psi_{n(k_t=0)} \middle| g^{(2)}{}_m \right\rangle^2\right] M_b{}^2$$

Where, $\left\langle \psi_{n(k_t=0)} \middle| g^{(1)}{}_m \right\rangle = \int_{-\infty}^{\infty} \psi_{n(k_t=0)}(z) g^{(1)}{}_m(z) dz$, M_b is the bulk average crystal momentum matrix that can be noted by:

$$M_b = (\frac{m_0}{m_e} - 1)\frac{m_0 E_g(E_g + \Delta)}{6(E_g + \frac{2}{3}\Delta)} \tag{25}$$

While, E_g and Δ are the energy band gap and split-off valence band separation respectively.

RESULTS AND DISCUSSIONS

Based on the mathematical model presented in Section 2, the crystal orientation-dependent optical properties of 8 nm Zinc-blende (ZB) $In_{0.1}Ga_{0.9}Sb$ QW architecture has been calculated. All the MATLAB simulation results have been shown in this paper considering the temperature at 300 K. The QW has been assumed to be 0.6% compressively strained due to the lattice mismatch between the well and GaAs substrate. The valence band dispersion curves obtained in [100], [110], [111] and [113] crystal orientations for the first Brillouin zone have been shown in Fig. 1(a)-(d). To compare the orientation-dependent energies, the figures are plotted as a function of wave vector in the same scale. It has been demonstrated, for a nonzero value of k (wave vector in the plain direction), the increasing conduction and spin-orbit split off band coupling gives rise to strong non-parabolicities in the valence band structure at [111] and [110] orientation. For [110] orientation, larger energy spacing between heavy hole and light hole band has been observed which will reduce the carrier density in the higher sub bands so effective mass of holes may reduce.

Since the QW is compressively strained, the maximum transition occurs between conduction band (C1) and heavy hole band (HH). The momentum matrix elements for transitions between C1 and HH in different crystal orientations have been measured and illustrated in Fig. 2. It is revealed that the optical matrix elements of non (001)-oriented QW structure rapidly decrease with increasing the wave vectors.

The maximum value of momentum matrix element is evaluated in (110) orientation and minimum in (131) orientation as the overlapping function of electrons and holes is maximum and minimum in (110) and (131) orientations, respectively.

In Fig 2(a) and (b), the graphical relationship has been depicted the dependence of hole effective mass Vs. well width (Lw) for the heavy (hh1) and light (lh1) holes with 3 nm≤Lw≤10 nm in $In_{0.1}Ga_{0.9}Sb$ QW. It has been noted that the mass decreased with well thickness increment. This is supported by the fact that the holes are confined in the barrier

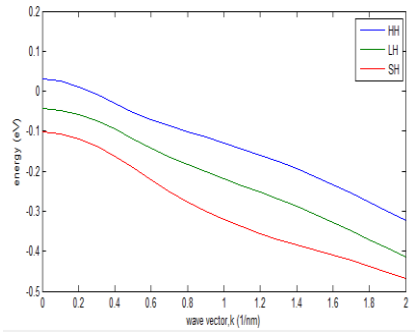

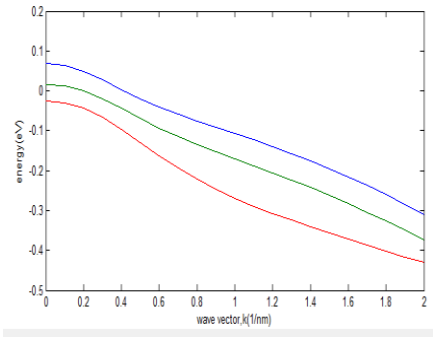

(b)

(a)

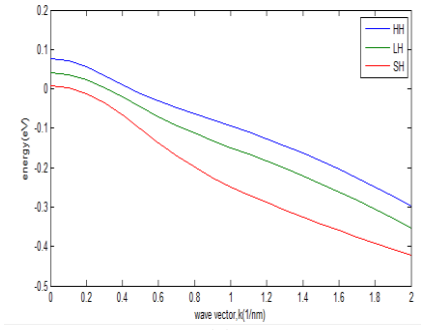

(e)

Fig. 1: Valence band dispersion profile of (a) 001 (b) 110 (c) 111 (d) 113 and (e) 131-oriented compressively strained $In_{0.1}Ga_{0.9}Sb$ QW.

where barrier width is fixed to 2 nm and the well width is varied. It has been found, due to minimum coupling between conduction and spin-orbit split off band in (110) crystal orientation, effective mass of hole is reduced which may lead to high mobility and peak drift velocity.

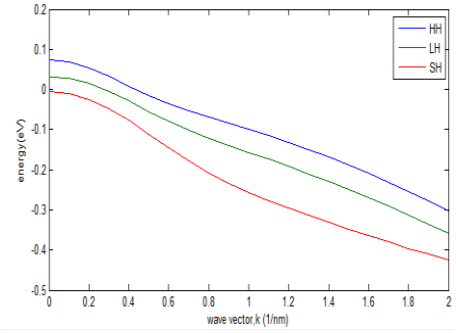

(c)

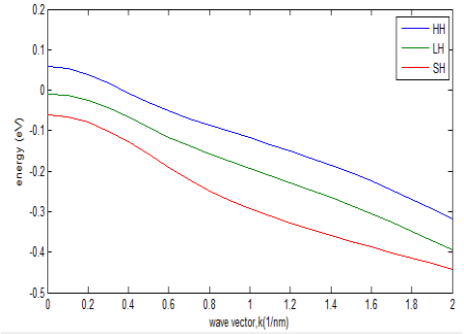

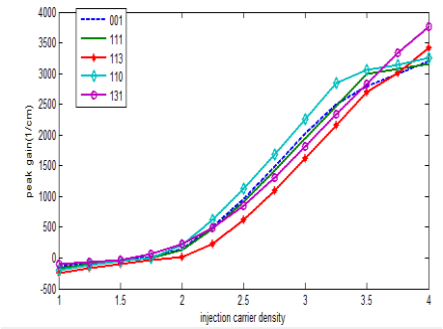

(a)

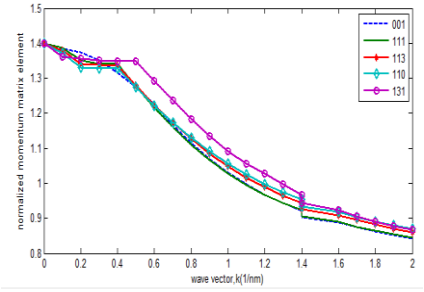

(b)

Fig. 2:(a) Carrier density dependent optical gain in different crystal orientations for 0.6% compressively strained ZB $In_{0.1}Ga_{0.9}Sb$ QW and (b) Crystal orientation-dependent normalized momentum matrix element

The optical gain spectra in different crystal orientations have been reckoned and shown in Fig. 3. The results have been figured out for injection carrier density of 2×10^{18} cm^{-3}.

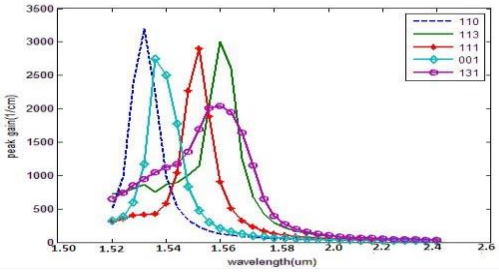

Fig. 3: optical gain evaluated in different crystal orientation for 0.6% compressively strained ZB $In_{0.1}Ga_{0.9}Sb$ QW

The amount of peak gain is assessed to be 2750 cm-1,3250 cm-1, 2800 cm-1, 2900 cm-1,and 1900 cm-1 in (001), (110), (111), (113) and (131) crystal orientations. The maximum gain has been checked out in (110) crystal orientation for wavelength 1550nm because the value of momentum matrix element for the transition from C1 to HH is higher in (1 1 0) orientation with respect to other orientation.

CONCLUSION

To recapitulate, the impact of crystal orientation on optical properties of compressively strained zinc-blend (ZB) $In_{0.1}Ga_{0.9}Sb$ QWs are theoretically investigated by practicing the multiband effective-mass theory. The theoretical results depict that the band mixing effect is minimum in (1 1 0) crystal orientation. The maximum gain and minimum threshold current density are also attained in (1 1 0) crystal orientation. This result regards that compressively strained (110) oriented ZB InGaSb/GaAs QW is a highly potential material for the fabrication of hetero-junction Laser for exclusive range of 1550 nm.

References

[1] T.Hausken, "The market for compound semiconductors in telecommunication networks," Compound Semiconductor, vol. 6, no. 3, pp. 23-27, 2000.
[2] R.S. Vodhanei, R.I. Laming, V. Shah, L. Curtis, D.P. Bour, W.L. Barnes, J.D. Mineally and F.J.Favire, "Highly efficient 978 nm diode-pumped erbium-doped amplifier with 24db gain," Electron. Lett., vol. 25, no. 20, pp. 1386-1388,1989.
[3] M.Yamida, M. Shimizu, T.Takeshita,M. Okayasu, M. Horiguchi, S. Uehara and E. Sugita, " Er^{+3} doped fiber amplifier pumped by 0.98 um laser diodes,"Photon. Technol. Lett., vol. 1,pp. 422-424, Dec. 1989.
[4] S.Shimada, "Impact of erbium-doped amplifiers on optical communication systems," Opt. Photon. News, vol. 1, no. 1,pp. 6-12,1990.
[5] H.C.Casey, Jr. and M.B. Panish, Heterostructure Lasers. Newyork: Academic, 1978.
[6] Y.A. Chang, J.R. Chen, H.C. Kuo, Y.K. Kuo, S.C. Wang, Theoretical experimental analysis on InAlGaAs/AlGaAs active region of 850-nm vertical-cavity surface emitting lasers, J. Lightwave Technol. 24 (2006), pp. 536–543.
[7] M. Phon, Y. Chung, W.I. Wang, Orientation dependence of valence-subband structures in GaAs–$Ga_{1-x}Al_xAs$ quantum well structures, J. Appl. Phys. 64 (1988) pp. 4609–4613.
[8] R.H. Henderson, E. Toweal, Strain and crystallographic orientation effects on interband optical matrix elements and band gaps of (1 1 1)-oriented III–V epilayers, J. Appl. Phys. 78 (1995) 2447–2455.
[9] R.H. Henderson, E.Toweal,Effective mass theory for III–V semiconductors on arbitrary (h k l) surfaces, J. Appl. Phys. 79 (1996) 2029–2037.
[10] G. Martin, A. Botchkarev, A. Rockett and H. Morko¸c, Appl. Phys. Lett. 68, 2541 (1996).
[11] F. Bernardini, V. Fiorentini and D. Vanderbilt, Phys. Rev. B 56, 10024 (1997).
[12] S. H. Park, J. Korean Phys. Soc. 50, 16 (2007).
[13] W. Fang and S. L. Chuang, Appl. Phys. Lett. 67, 751 (1995).
[14] K. Domen, K. Horino, A. Kuramata and T. Tanahashi, Appl. Phys. Lett. 70, 987 (1997).
[15] A. Niwa, T. Ohtoshi and T. Kuroda, Appl. Phys. Lett. 70, 2159 (1997).
[16] S. H. Park and S. L. Chuang, Phys. Rev. B 59, 4725 (1999).
[17] T. Takeuchi,H. Amano and I.Akasaki, Japan. J. Appl.Phys. 39,413 (2000).
[18] F. Mireles and S. E. Ulloa, Phys. Rev. B 62, 2562 (2000).
[19] S. H. Park, J. Appl. Phys. 91, 9904 (2002).
[20] T. Ohtoshi, A. Niwa and T. Kuroda, IEEE J. Select. Topics Quantum Electron. 4, 527 (1998).
[21] S.L. Chuang, Physics of Optoelectronics Devices, John Wiley & Sons, 1995.
[22] G.R. Nash, S.J. Smith, S.D. Coomber, S. Przeslak, A. Andreev, P. Carrington, M. Yin, A. Krier, L. Buckle, M.T. Emeny, T. Ashley, Mid-infrared GaInSb/AlGaInSb quantum well laser diode grown on GaAs, Appl. Phys. Lett. 91 (2007), 131118(1–3).
[23] A. Niwa, T. Ohtoshi, T. Kuroda, Orientation dependence of optical properties in long wavelength strained quantum-well lasers, IEEE J. Selected Top. Quantum Electron. 1 (1995) 211–217.
[24] Y. Okuno, K. Uomi, M. Aoki, T. Tsuchiya, Direct wafer bonding of III–V compound semiconductors for free-material

and free-orientation integration, IEEE J. Quantum Electron. 33 (1997) 959–969.
[25] T. Ohtoshi, T. Kuroda, A. Niwa, S. Tsuji, Dependence of optical gain on crystal orientation in surface-emitting lasers with strained quantum wells, Appl. Phys. Lett. 65 (1994) 1886–1889.
[26] S.L. Chuang, Physics of Optoelectronics Devices, John Wiley & Sons, 1995.

.